Article

Interdecadal modulation of Ningaloo Niño/ Niña strength in the Southeast Indian Ocean by the Atlantic Multidecadal Oscillation

Jiaqing Xue [1,2,3] ✉, Wenjun Zhang [1,2] ✉, Yutong Zhang[1,2], Jing-Jia Luo [1,3], Hualong Zhu[1,2], Cheng Sun [4] & Toshio Yamagata [5]

The Southeast Indian Ocean is a global hotspot for marine heatwaves. In that region, marine heatwaves/cold-spells are known as Ningaloo Niño/Niña events, and have substantial impacts on regional climate anomalies and unique marine ecosystems. However, the strength of Ningaloo Niño/Niña events is nonstationary and varies considerably at multidecadal timescales. Here we find that the interdecadal fluctuations in Ningaloo Niño/Niña strength are modulated by the Atlantic Multidecadal Oscillation (AMO), with strengthened (weakened) Ningaloo Niño/Niña corresponding to a positive (negative) AMO phase. During the positive AMO phase, the Atlantic warm sea surface temperature (SST) anomalies drive a series of climate mean-state changes in the Indo-Pacific region through tropics-wide teleconnections, including SST cooling over the central Pacific and SST warming in the tropical eastern Indian Ocean. Those mean-state changes tend to enhance El Niño-Southern Oscillation (ENSO)-related atmospheric and oceanic teleconnections to the Southeast Indian Ocean, and increase local Indian Ocean ocean–atmosphere coupling, promoting the Ningaloo Niño/Niña growth. Our findings highlight the critical role of the remote influence of AMO in understanding the Southeast Indian Ocean marine heatwaves/cold-spells and associated climatic and socioeconomic impacts.

Marine heatwaves have recently attracted considerable scientific and public attention due to their devastating impacts on marine ecosystems and the economics of regional fisheries. Especially, these extreme events are expected to increase in frequency, intensity and duration under continued global warming[1–3]. The Southeast Indian Ocean, a transition zone between tropical and temperate biota with unique marine biodiversity and atoll coral reefs, has become a global hotspot for marine heatwave research. Over there, marine heatwaves/cold-spells are also dubbed Ningaloo Niño/Niña, which is the dominant mode of interannual climate variability in the southeastern Indian Ocean[4–9]. The

Ningaloo Niño/Niña is characterized by warm/cold sea surface temperature (SST) anomalies off the west coast of Australia, developing in austral spring and reaching the peak in austral summer[10,11] (Supplementary Fig. 1). Two key mechanisms, which are not mutually exclusive, have been proposed to explain the generation of Ningaloo Niño/Niña. Those are remote forcing from El Niño-Southern Oscillation (ENSO) and local ocean–atmosphere–land interactions over the Southeast Indian Ocean[12–15]. The Ningaloo Niño/Niña is strongly correlated with the SST variability in equatorial western-central Pacific (Niño-4W) region[16,17] (Supplementary Fig. 2). The ENSO contributes to the development of

[1]State Key Laboratory of Climate System Prediction and Risk Management/Key Laboratory of Meteorological Disaster, Ministry of Education/Collaborative Innovation Center on Forecast and Evaluation of Meteorological Disasters, Nanjing University of Information Science and Technology, Nanjing, China. [2]School of Atmospheric Sciences, Nanjing University of Information Science and Technology, Nanjing, China. [3]Institute for Climate and Application Research, Nanjing University of Information Science and Technology, Nanjing, China. [4]State Key Laboratory of Remote Sensing Science, Faculty of Geographical Science, Beijing Normal University, Beijing, China. [5]Application Laboratory/Research Institute for Value-Added-Information Generation, Japan Agency for Marine-Earth Science and Technology, Yokohama, Japan. ✉e-mail: xjq@nuist.edu.cn; zhangwj@nuist.edu.cn

Ningaloo Niño/Niña via both atmospheric bridge and oceanic pathway. A Matsuno–Gill-type response to La Niña related diabatic heating anomalies induce negative sea level pressure anomalies over the Southeast Indian Ocean. The associated northerly alongshore wind anomalies generate Ningaloo Niño by strengthening the poleward warm advection by Leeuwin Current and suppressing the coastal upwelling and latent heat loss. Meanwhile, the easterly wind anomalies associated with La Niña over the tropical Pacific produce downwelling equatorial Rossby waves, which penetrates through the Indonesian Throughflow and propagate poleward along the west coast of Australia as coastal downwelling Kelvin waves. These coastal oceanic long waves strengthen the Leeuwin Current, giving rise to development of Ningaloo Niño[7,13,14]. In addition, the local ocean–atmosphere–land interactions called the coastal Bjerknes feedback may operate to induce Ningaloo Niño/Niña events as well. The positive feedback loop can be expressed as follows. Suppose that warm SST anomalies are somewhat generated off the western Australia, which may induce low atmospheric pressure anomalies aloft. The atmospheric pressure difference between the ocean and the continent leads to northerly wind anomalies, which may reinforce the initial SST anomalies through suppressing latent heat loss and coastal upwelling and enhancing the Leeuwin Current[18–21]. The mirror image above may explain the evolution of Ningaloo Niña events.

As the dominant interannual climate mode of the Southeast Indian Ocean, Ningaloo Niño/Niña can strongly modulate atmospheric circulations and affect local climate variations, with Ningaloo Niño (Niña) corresponding to increased (decreased) precipitation and surface air temperature off the Western Australia[8,22,23]. In addition to being forced by ENSO, the Ningaloo Niño could also actively influence the tropical Pacific climate. The SST anomalies associated with the Ningaloo Niño induces negative sea level pressure anomalies extending from the southeastern Indian Ocean to the Maritime Continent, which strengthens the trade winds, and therefore cools the central tropical Pacific due to enhanced equatorial upwelling[24]. More importantly, the Ningaloo Niño/Niña region, listed as World Heritage area by the United Nations, is home of not only highly productive but also fragile marine ecosystems; the occurrence of Ningaloo Niño/Niña events hence exerts prominent impacts on ocean biodiversity. For instance, the unprecedented Southeast Indian Ocean marine heatwave associated with the 2011 extreme Ningaloo Niño severely damaged local fisheries and coral reefs[7,25–27]. Actually, this incident drew attention to the Ningaloo Niño and stimulated active research under the name of this newly catalogued phenomenon[8]. In view of its widespread impacts, a better understanding of Ningaloo Niño/Niña change is hence of great societal and scientific importance.

The Ningaloo Niño/Niña exhibits certain nonstationary features with prominent interdecadal variations. For example, the Ningaloo Niño events occur more frequently during 1960s and after late 1990s. Such frequent occurrences were suggested to be linked to the negative phase of the Interdecadal Pacific Oscillation (IPO), which may enhance poleward warm advection by the Leeuwin Current through anomalous strengthening of the Indonesian Throughflow and cyclonic wind anomalies off the west coast of Australia, favoring the development of Ningaloo Niño events[28,29]. Different from the situation of frequency modulation, the overall relationship between IPO and the decadal variation of Ningaloo Niño/Niña amplitude is weak, although IPO may have some contribution for the post-1980 period[29] (Supplementary Fig. 3a). Accordingly, the IPO cannot well explain the decadal variations in Ningaloo Niño/Niña amplitude, and further investigations into the decadal modulation of Ningaloo Niño/Niña strength is needed.

In addition to the IPO, the Atlantic Multidecadal Oscillation (AMO), characterized by spatially coherent SST anomalies across the North Atlantic basin, is another important interdecadal climate mode[30]. The persistent basin-scale SST anomalies associated with the AMO not only influence climate over the surrounding continents, but also act as a key pacemaker for Indo-Pacific climate variations on

interdecadal timescales[31–36]. Previous studies have demonstrated that the AMO can force the North Pacific and western tropical Pacific interdecadal variability via the extratropical atmospheric bridge, and drives IPO-like pattern in the tropical Pacific by altering Walker circulation[37–41]. Meanwhile, through the atmospheric teleconnections, the AMO also exerts strong interdecadal impacts on Indian Ocean rim climate, including tropical Indian Ocean SST, Indian monsoon rainfall, and so on[40,42]. Recently, the AMO is further found to modulate the Indo-Pacific inter-basin connections. The warm phases of the AMO tend to weaken the inter-basin connection between ENSO and the Indian Ocean Dipole, which are two most important interannual climate signals with worldwide climate and socioeconomic impacts[43].

Despite many previous studies on the Atlantic and Indo-Pacific connections, it is still unclear whether there is a close relationship between AMO and the decadal variation of Ningaloo Niño/Niña strength. The related knowledge is of great importance for predicting the future variability of Ningaloo Niño/Niña and informing decision-making on potential risks of extreme events in the warming climate. In this study, we find that the observed interdecadal variations in Ningaloo Niño/Niña amplitude are closely linked to the AMO based on observational analyses and modelling experiments.

Results

Interdecadal modulation of Ningaloo Niño/Niña strength

Since Ningaloo Niño/Niña develops in austral spring and reaches its peak in the January–March (JFM) season[44] (Supplementary Fig. 1b), the JFM Ningaloo Niño/Niña index (NNI) is hence used to measure its strength. Figure 1a first shows the time series of JFM NNI during 1920–2018. It is noted that the amplitude of Ningaloo Niño/Niña seems to be nonstationary, with interdecadal variations. To demonstrate this, Fig. 1b investigates the 21-year sliding interannual standard deviation of JFM NNI based on the ERSST v5 dataset (red line). Indeed, the strength of Ningaloo Niño/Niña displays remarkable interdecadal fluctuations with a strong intensity from the 1930s to 1950s and after the 2000s, and with a weak intensity roughly from the 1960s to 1990s. Existing studies have demonstrated the essential roles of AMO and IPO in driving the climate variability on interdecadal timescales[31,32,45,46]. To examine the possible linkage of the decadal variations of Ningaloo Niño/Niña strength with these decadal variability modes, we calculate the correlation of decadal variation of Ningaloo Niño/Niña strength with the decadal SST variability, which is measured by 11-year running mean annual SST anomalies (Fig. 1c). The pattern is characterized by significant positive correlations across the North Atlantic basin, suggesting a close statistical relationship with the remote AMO. The time evolution of normalized AMO index is compared with that of Ningaloo Niño/Niña strength in Fig. 1b. Amazingly, the decadal variations of Ningaloo Niño/Niña strength are highly in phase with that of AMO, with strengthened (weakened) Ningaloo Niño/Niña corresponding to AMO positive (negative) phases. The correlation coefficient between them reaches as high as 0.84. This relationship is demonstrated to be robust and unaffected by the choice of SST datasets (Supplementary Fig. 4). To further confirm whether such relationship exists for both Ningaloo Niño and Ningaloo Niña, we categorize Ningaloo Niño/Niña events into four types based on different AMO phases, that is, Ningaloo Niño during positive AMO (Ningaloo Niño/AMO+), Ningaloo Niño during negative AMO (Ningaloo Niño/AMO−), Ningaloo Niña during positive AMO (Ningaloo Niña/AMO+), and Ningaloo Niña during negative AMO (Ningaloo Niña/AMO−). Here, time periods when the 11-year running mean AMO index is greater than (less than) 0 are identified as AMO+ (AMO−). As displayed in Fig. 1d, both Ningaloo Niño and Ningaloo Niña events are intensified during the positive AMO phase compared with those during the negative AMO phase, and their differences are significant at the 95% and 90% confidence level respectively. While for the IPO, no statistically significant relationship is found with the Ningaloo
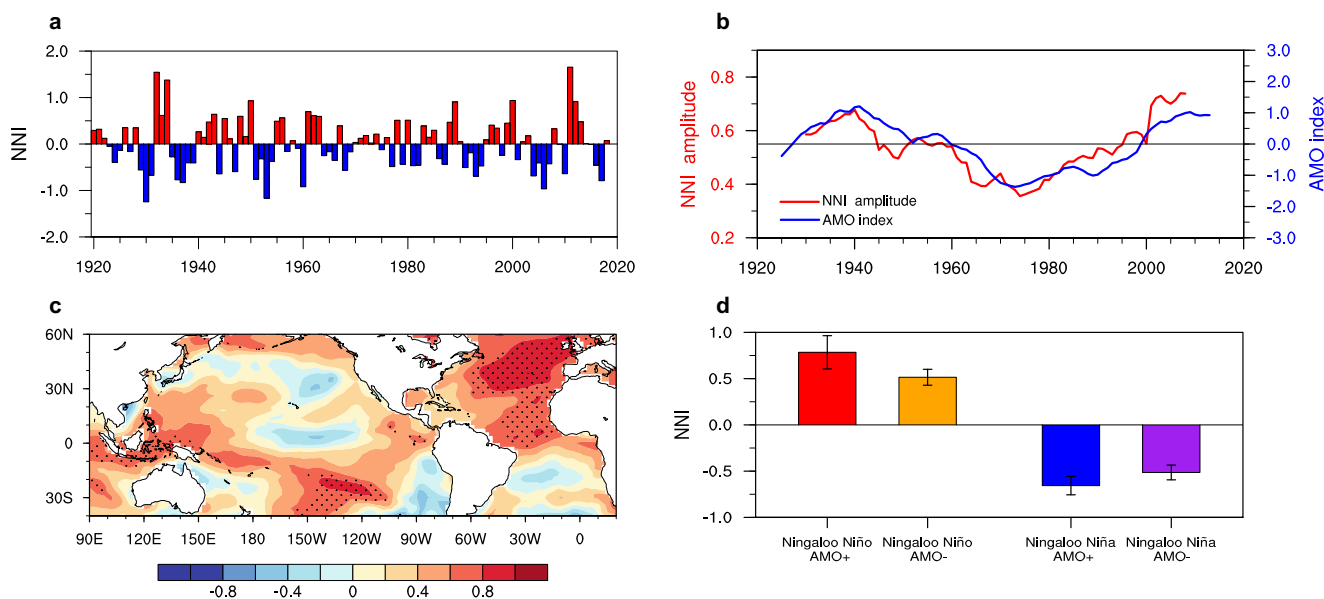
Fig. 1 | Relationship between Ningaloo Niño/Niña strength and the Atlantic Multidecadal Oscillation (AMO). a The time series of January–March (JFM) Ningaloo Niño/Niña index (NNI; bar; °C) during 1920–2018. **b** Decadal variation of Ningaloo Niño/Niña strength as measured by the detrended 21-year sliding inter-annual standard deviation of JFM NNI (red line; °C) and the 11-year running mean normalized AMO index (blue line). **c** Correlation map between the decadal variations of Ningaloo Niño/Niña strength and the decadal annual sea surface temperature (SST) anomalies during the period 1920–2018. The dotted shading indicates correlations that are statistically significant at the 90% confidence level. **d** Composite JFM NNI (bar; °C) for AMO+/Ningaloo Niño (red), AMO–/Ningaloo Niño (orange), AMO+/Ningaloo Niña (blue) and AMO-/Ningaloo Niña (purple). The Ningaloo Niño (Niña) events are selected if the JFM NNI is greater (less) than 0.6 (−0.6) standard deviation. The positive AMO indicates the 1928–1959 and 1999–2018 periods, negative AMO indicates the 1920–1927 and 1960–1998 periods. Error bars indicate the 90% confidence intervals.

Niño/Niña strength. The correlation coefficient between their time evolutions is only 0.04 (Supplementary Fig. 3).

As Ningaloo Niño/Niña events can be generated by both remote ENSO forcing and local ocean–atmosphere interactions, it is expected that the AMO could have impacts on Ningaloo Niño/Niña strength by modulating the ENSO teleconnections or local air–sea coupling in the Indian Ocean. Firstly, the interdecadal variation of ENSO related Ningaloo Niño/Niña variability is investigated in Supplementary Fig. 5. The evolution is found to be very consistent with that of Ningaloo Niño/Niña amplitude, which indicates that part of decal variations in Ningaloo Niño/Niña strength can be ascribed to changes in ENSO teleconnections between different AMO phases. Figure 2 presents the observed Indo-Pacific signature of La Niña in the positive phase of the AMO from 1999 to 2018. During La Niña, the atmospheric convection is suppressed over the central equatorial Pacific and enhanced over the western equatorial Pacific. The associated positive diabatic heating anomalies over the western Pacific generate an anomalous cyclonic circulation over the Southeast Indian Ocean through the Matsuno–Gill-type response, which corresponds to alongshore northerly wind anomalies off the western coast of Australia, leading to coastal SST warming by suppressing coastal upwelling and latent heat loss (Fig. 2a). Meanwhile, the easterly wind anomalies over the equatorial Pacific induced by La Niña trigger the westward propagating down-welling Rossby wave in the ocean, which intrude into the Indian Ocean via the Indonesian Throughflow and propagate poleward along the western coast of Australia as coastal Kelvin waves (Fig. 2b). Those downwelling waves also act to warm coastal SST by enhancing pole-ward warm advection by Leeuwin Current. As such, the La Niña leads to the development of Ningaloo Niño events through both atmospheric and oceanic teleconnections (Fig. 2c). For comparison, the ENSO teleconnections in the negative phase of the AMO during 1960–1998 are examined in Fig. 2d–f. Accompanying the weakening of ENSO teleconnections, the La Niña induced Ningaloo Niño in AMO negative phase is clearly weaker than that in AMO positive phase (Fig. 2g–i).

Similarly, the signature of AMO on local ocean–atmosphere interactions in the Indian Ocean is also investigated for the case of Ningaloo Niño development. Figure 3a–d shows the ocean–atmosphere coupled anomalies of Ningaloo Niño in AMO positive phase, obtained by regressing JFM SST, precipitation, low-level atmospheric circulation and sea surface height (SSH) onto the un-normalized NNI during 1999–2018. As depicted in the coastal Bjerknes feedback loop, warm coastal SST anomalies associated with the Ningaloo Niño enhances atmospheric convection off the Northwest Australia, which generate an anomalous cyclone over the southeast Indian Ocean by heating the atmosphere. The anomalous cyclone give rise to southward alongshore wind anomalies, which suppress coastal upwelling and strengthens the warm advection of the Leeuwin Current, amplifying the initial SST anomalies. As a comparison, the ocean–atmosphere coupling of Ningaloo Niño in AMO negative phase is analyzed in Fig. 3e–h. It is noted that Ningaloo Niño SST anomalies are more effective in enhancing atmospheric convection during positive AMO, the associated alongshore wind and SSH anomalies are hence stronger than those during the negative AMO (Fig. 3i–l). To focus only the local air–sea coupling which is independent of ENSO, we further compare the coastal Bjerknes feedback between different AMO phases with the simultaneous ENSO signal being linearly removed. Even excluding the ENSO influences, the results remain basically the same (Supplementary Fig. 6). The above results are based on linear analyses, so the mirror images correspond to the Ningaloo Niña situations. Therefore, we may conclude that the strengthened ENSO teleconnections and local ocean–atmosphere feedback contributes to the enhanced Ningaloo Niño/Niña amplitude during positive AMO.

AMO induced Indo-Pacific background state changes

To understand why ENSO teleconnections and Indian Ocean local ocean–atmosphere feedback change with the AMO phases, the footprints of AMO on the Indo-Pacific mean climate are further explored (Fig. 4). The analyses focus on the period from October to March when
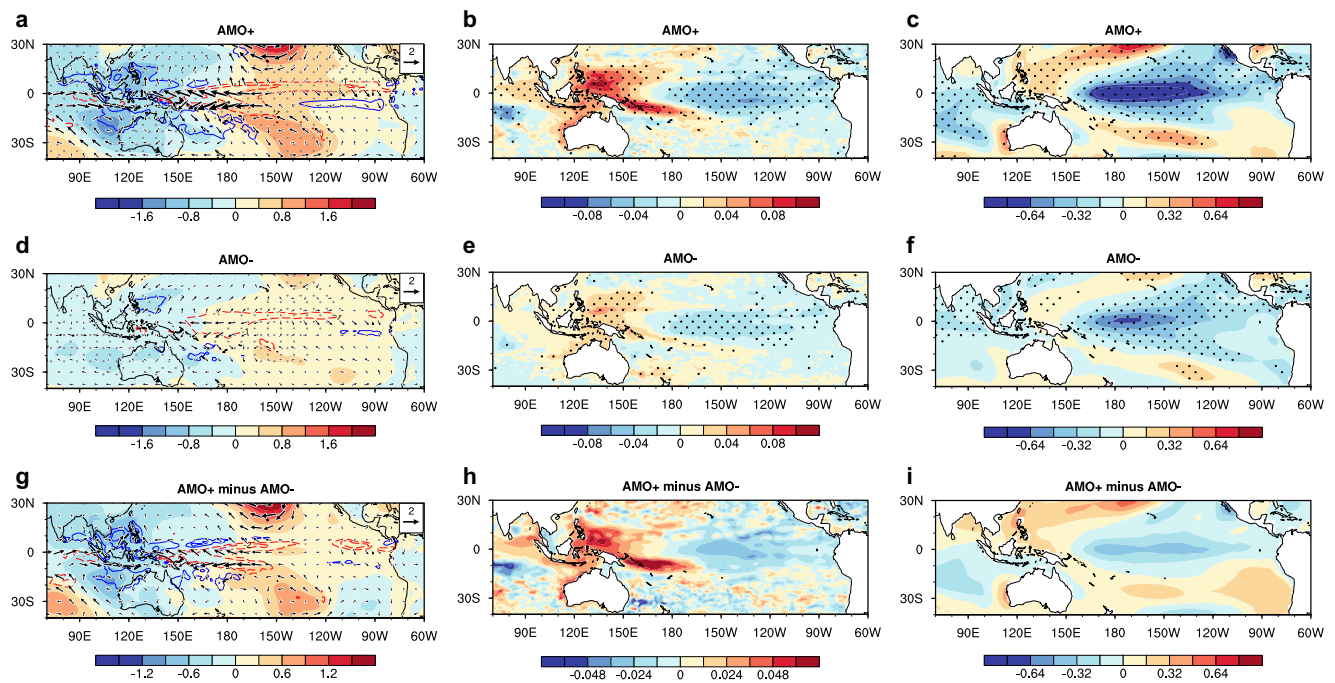
Fig. 2 | Observed differences in El Niño-Southern Oscillation teleconnections between the positive and negative phases of the Atlantic Multidecadal Oscillation (AMO). a–c Regression maps of the interannual anomalies of January–March (JFM) (**a**) sea level pressure (shading; hPa), 925-hPa wind (vectors; m s^{-1}), precipitation (contours; mm day^{-1}), (**b**) sea surface height (m), and (**c**) sea surface temperature (°C) with respect to the normalized reversed JFM Niño-4W index in the positive phase of the AMO during 1999–2018. **d–f** As in (**a–c**), but in the negative phase of the AMO during 1960–1998. **g–i** Differences of the regression patterns between the positive and negative AMO. The dotted shading denotes regressions that are statistically significant at the 95% confidence level.

Ningaloo Niño/Niña develops and peaks. The results indicate that positive AMO is accompanied by mean SST cooling over the equatorial central Pacific and mean SST warming over the Indo-western Pacific (Fig. 4a). Those tropical SST anomalies are interconnected through the zonal Walker circulation in the atmosphere. The tropical Atlantic warming associated with the positive AMO accelerates the Pacific Walker circulation through both boundary layer heating and upper-level convective heating, leading to anomalous ascent over the tropical Atlantic and anomalous descent over the central Pacific. At the surface, this circulation change is manifested as easterly wind anomalies from the central to western tropical Pacific (Fig. 4b–d). Accompanying the anomalous surface winds, ocean thermocline is anomalously tilted, showing subsurface cooling (warming) in the eastern (western) Pacific (Fig. 4e, f). As such, central-eastern Pacific SST is cooled due to enhanced surface evaporation, Ekman pumping and shoaled thermocline, while the western Pacific SST is warmed by enhanced ocean zonal advection and deepened thermocline. Once the western Pacific is warmed, it can lead to enhanced convection and associated diabatic heating, which drives anomalous westerly wind over the tropical Indian Ocean, and reinforces the Atlantic induced anomalous easterly wind over the equatorial Pacific. The results also indicate that the influence of AMO on Indian Ocean is primarily through the western Pacific warming, which overwhelms the direct influence from the Atlantic through Gill-type response. The westerly wind anomalies over the tropical Indian Ocean deepens the mean thermocline depth over the eastern Indian Ocean, leading to the SST warming there (Fig. 4d–f).

These AMO induced mean-state changes further influence the interannual ocean–atmosphere interactions, thereby modulating the Ningaloo Niño/Niña strength. Figure 5a, b present the standard deviation of November–January (NDJ) and JFM SST anomalies over the tropical Pacific in positive phase of the AMO during 1999–2018. In contrast, Fig. 5c, d show the standard deviation of SST anomalies in negative phase of the AMO. Obviously, the center of ENSO related SST variability show a westward shift during positive AMO compared to that during

negative AMO, leading to increased SST variability over the equatorial western-central Pacific (Fig. 5e, f). Such changes in ENSO pattern can be ascribed to the AMO induced tropical Pacific background state changes. As demonstrated in previous studies, the La Niña-like interdecadal cooling associated with AMO could favor more frequent occurrence of central Pacific-type (Modoki-type) ENSO[47–50]. It is observed that the frequency of central Pacific-type ENSO has nearly doubled during recent AMO positive phase compared with the previous negative phase (Supplementary Fig. 7). This is because the increased background SST gradient shift the anomalous convection and wind responses westward from the underlying SST forcing, therefore leading to the westward shift of ENSO center. In addition to modulating the properties of ENSO itself, the mean state changes also influence the Indian Ocean sensitivity to ENSO forcing, which can be measured by the regressions onto the un-normalized Niño-4W index (Supplementary Fig. 8). As seen in the figure, La Niña induced convection response over the Maritime continent during positive AMO are greater than those during negative AMO for a given 1-degree SST anomaly forcing. This is because mean SST warming over the western Pacific enhances local mean atmospheric specific humidity, which amplifies the convection response to ENSO forcing by enhancing moisture convergence or divergence (Supplementary Fig. 9). Accompanying this, same La Niña forcing generates stronger southward alongshore wind and positive SSH anomalies off the Western Australia during positive AMO than those during negative AMO, therefore resulting in warmer coastal SST anomalies. Consequently, AMO modulates the influence of ENSO on Ningaloo Niño/Niña by changing both the ENSO pattern and the Indian Ocean sensitivity to ENSO forcing. As for the coastal Bjerknes feedback, its strength is also subject to the AMO modulation. In positive phase of the AMO, the tropical eastern Indian Ocean SST is anomalously warmed. The intensified heating below thus leads to more unstable atmosphere and enhanced local convection (Fig. 4a, b). During this unstable and convection-active period, atmospheric convection will be more sensitive to underlying SST anomalies. Aa a result, we can see in Fig. 3 that 1-degree Ningaloo
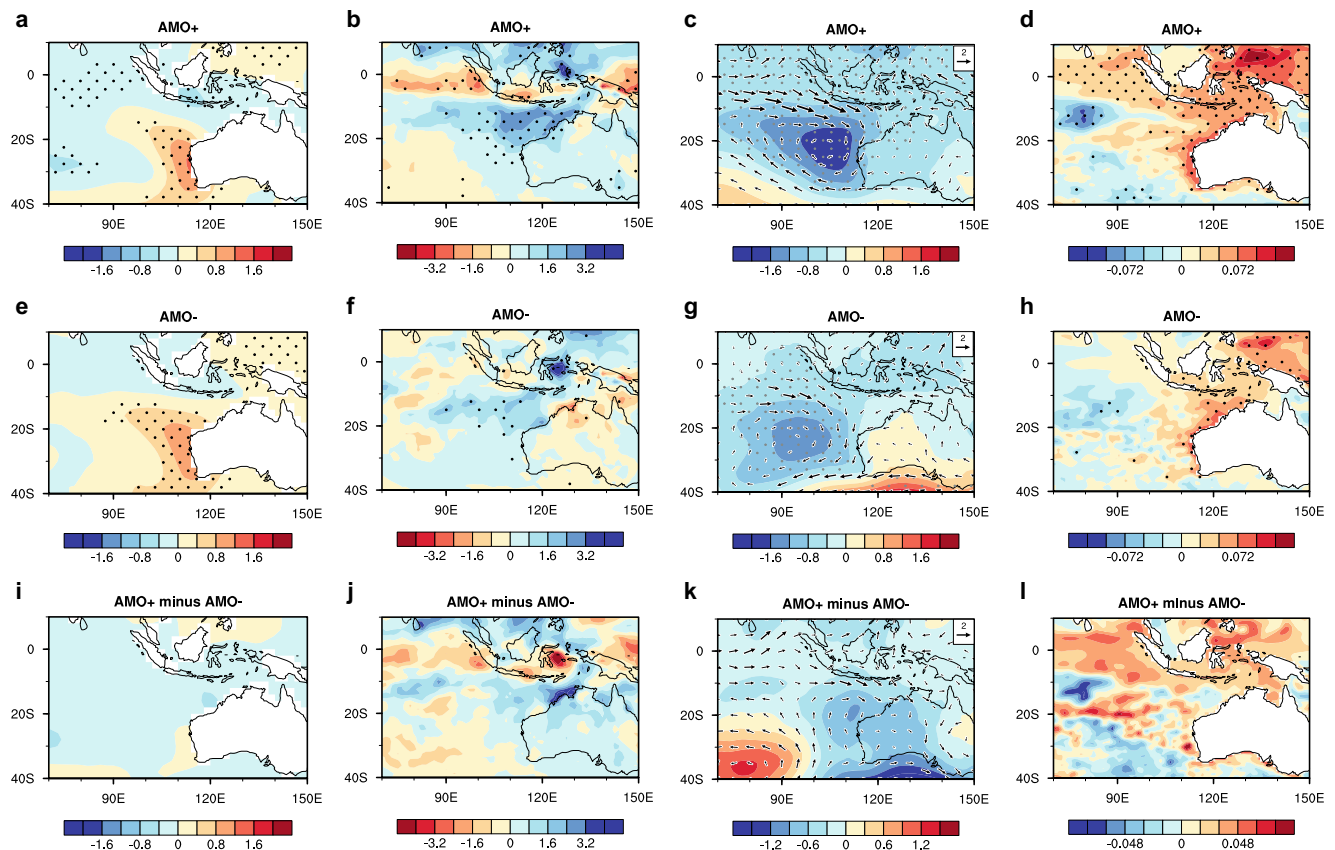
Fig. 3 | Observed differences in the local Indian Ocean ocean–atmosphere feedback between the positive and negative Atlantic Multidecadal Oscillation (AMO). **a–d** Regression maps of the interannual January–March (JFM) (**a**) sea surface temperature (°C), (**b**) precipitation (mm day^{-1}), (**c**) sea level pressure (shading; hPa) and 925-hPa wind (vectors; m s^{-1}), (**d**) sea surface height (m) anomalies onto the un-normalized Ningaloo Niño/Niña index (NNI) in the positive phase of the AMO during 1999–2018. **e–h** As in (**a–d**), but in the negative phase of the AMO during 1960–1998. **i–l** Differences of the regression patterns between the positive and negative AMO. The dotted shading denotes regressions that are statistically significant at the 95% confidence level.

Niño/Niña SST anomalies generate stronger convection anomalies during positive AMO, which are responsible for the enhanced strength of coastal Bjerknes feedback over the Southeast Indian Ocean, generating stronger Ningaloo Niño/Niña.

Idealized Atlantic pacemaker experiments

The above observational analyses indicate that the AMO may modulate Ningaloo Niño/Niña strength by modifying Indo-Pacific mean climate and interannual ocean–atmosphere interactions. To further confirm this, a suit of idealized Atlantic pacemaker experiments based on the EC-Earth3 Earth System Model is used. The experiments, run with time-independent AMO SST anomalies prescribed only in the North Atlantic and with free ocean–atmosphere interactions in other ocean basins, demonstrate the AMO forcing on Indo-Pacific climate variability (see Methods for details). Figure 6a, b shows the Ningaloo Niño/Niña patterns for AMO+ and AMO− simulations, respectively. The modeling results demonstrate that AMO can indeed modulate Ningaloo Niño/Niña strength, with Ningaloo Niño/Niña amplitude for AMO+ being larger than that for AMO− (Fig. 6c). Specifically, the standard deviation of JFM NNI is 0.65 in AMO+ simulations and 0.55 in AMO− simulations, the difference in standard deviations is significant at the 95% confidence level. The modulation is also reflected in the power spectrums of NNI, the interannual Ningaloo Niño/Niña variability for AMO+ simulations are observed to be much stronger than that for AMO− simulations (Supplementary Fig. 10). Moreover, the composite JFM NNI for AMO+/Ningaloo Niño, AMO−/Ningaloo Niño, AMO+/Ningaloo Niña and AMO−/Ningaloo Niña in idealized Atlantic pacemaker experiments are examined. Consistent with the observational results,

Ningaloo Niño and Ningaloo Niña events are intensified in positive AMO compared with those in negative AMO, their differences both are significant at the 95% confidence level (Fig. 6d).

Since AMO is suggested to modulate Ningaloo Niño/Niña by changing Indo-Pacific mean climate, the footprints of AMO on the Indo-Pacific background state are also verified in idealized Atlantic pacemaker experiments (Supplementary Fig. 11). It is observed that the AMO induced mean-state changes over the Indo-Pacific region in pacemaker simulations are basically consistent with the observations. Accompanying the mean-state changes, the ENSO teleconnections and local Indian Ocean ocean–atmosphere interactions are strengthened accordingly (Supplementary Figs. 12–14). Therefore, the coupled model experiments further support the AMO modulation of Ningaloo Niño/Niña strength by modifying the Indo-Pacific mean state and interannual ocean–atmosphere interactions. Although the simulated responses shown above are consistent with the observations, it is noted that the simulated intensity is somewhat weaker than the observational results. Such differences may be explained by the climatological SST bias in model over the North Atlantic. The colder climatological background state could reduce the anomalous responses to the AMO SST forcing (Supplementary Fig. 15).

Discussion

The Ningaloo Niño/Niña events, corresponding to Southeast Indian Ocean marine heatwaves/cold-spells, are found to exhibit a nonstationary feature with prominent interdecadal fluctuations in strength, undergoing strong periods from the 1930s to 1950s and after the
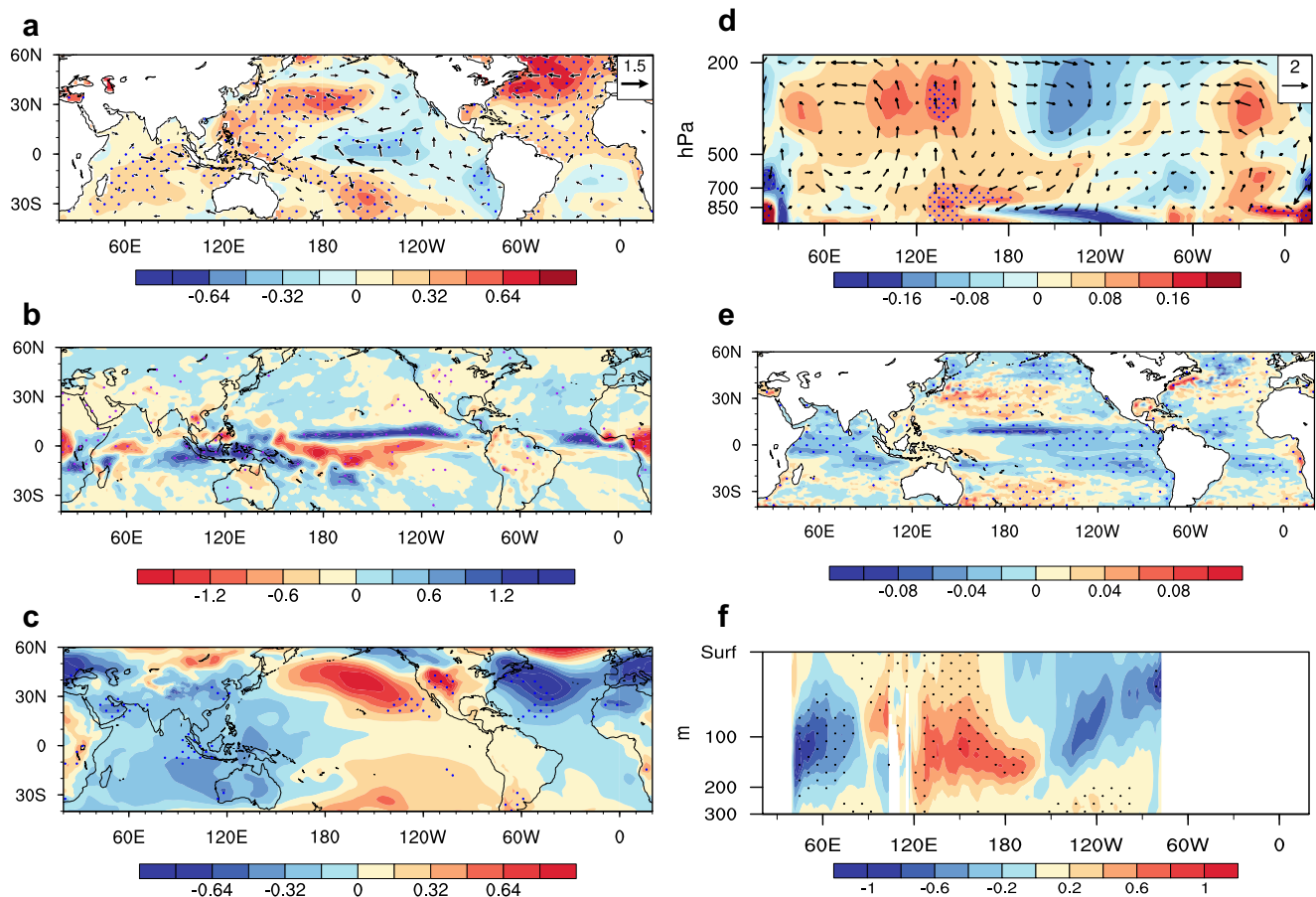
Fig. 4 | The footprints of Atlantic Multidecadal Oscillation (AMO) on Indo-Pacific coupled ocean–atmosphere system in observations. Difference maps of the anomalous (**a**) sea surface temperature (shading; °C) and 925-hPa winds (vectors; m s⁻¹), (**b**) precipitation (mm day⁻¹), (**c**) sea level pressure (hPa), (**d**) equatorial tropospheric air temperature (shading; °C) and Walker circulation (vectors; m s⁻¹) averaged over 5°S–5°N, (**e**) sea surface height (m), (**f**) Indo-Pacific Ocean subsurface temperature (°C) averaged over 5°S–5°N between the positive AMO during 1999–2018 and the negative AMO during 1960–1998. The variables are averaged from October to March of the next year. The vertical velocity is magnified by a factor of −100 to make it comparable to the zonal winds. Dotted shading indicates the differences that are statistically significant at the 90% confidence level.

2000s, and a weak period from 1960s to 1990s. We have shown that the AMO acts as a key pacemaker for Ningaloo Niño/Niña amplitude, with AMO positive (negative) phases corresponding to strengthened (weakened) Ningaloo Niño/Niña. Figure 7 provides a schematic diagram summarizing the physical processes through which the AMO modulates the Ningaloo Niño/Niña strength. Via the atmospheric Walker circulation, the tropical Atlantic warming associated with the positive AMO drives a series of Indo-Pacific mean-state changes, including mean SST cooling over the central Pacific and mean SST warming in the tropical eastern Indian Ocean (Fig. 7a). The Indo-Pacific mean-state changes further modulate both ENSO teleconnections to the Southeast Indian Ocean and local Indian Ocean ocean–atmosphere coupling, thereby exerting a substantial impact on the Ningaloo Niño/Niña strength (Fig. 7b, c). These findings highlight the critical role of the remote influence of AMO in marine heatwave/cold-spells evolution over the Southeast Indian Ocean, advancing our understandings on inter-basin and cross-scale interactions between the Atlantic and Indo-Pacific Oceans. Based on the present findings, we expect that more marine heatwaves/cold-spells off the Western Australian coast may occur under the current AMO positive phase. Policymakers need to be vigilant about this, and prepared for the potential risks.

Although there is an anti-phase relationship between IPO and Ningaloo Niño/Niña amplitude for the post-1980 period, the overall modulation of IPO on Ningaloo Niño/Niña strength is weak over a longer period. Neither Ningaloo Niño nor Ningaloo Niña strength show

significant differences between different IPO phases (Supplementary Fig. 3). To figure out why the IPO influence is so weak, we compare the changes of ENSO teleconnections to the Southeast Indian Ocean and local Indian Ocean ocean–atmosphere coupling with the IPO phases. Distinct from the situation of AMO, the ENSO teleconnections and local ocean–atmosphere coupling both change little with the IPO phases (Supplementary Figs. 16 and 17). This could be further explained by the footprints of IPO on Indo-Pacific mean climate. Different from the positive AMO induced central Pacific cooling, the negative IPO is accompanied by mean SST cooling over the eastern Pacific, which corresponds to the weakening rather than westward shift of ENSO. In this case, the IPO cannot have significant impacts on SST variability in the Niño-4W region as the AMO can, which explains why ENSO teleconnections change so little with the IPO phases. For the tropical eastern Indian Ocean, the footprints of IPO on SST and convection are weak as well, which are responsible for the weak modulation of IPO on the coastal Bjerknes feedback (Supplementary Figs. 18 and 19). Accordingly, different form the AMO, the IPO is demonstrated to have a relatively weak influence on Ningaloo Niño/Niña amplitude. Recent study indicates the Ningaloo Niño/Niña region itself also exhibits strong decadal SST variability[16]. Although its correlation with the decadal variations of Ningaloo Niño/Niña amplitude is very weak (Fig. 1c), we cannot exclude the possibility that it may modulate Ningaloo Niño/Niña strength in a complex nonlinear way, this is worthy of further study in the future.
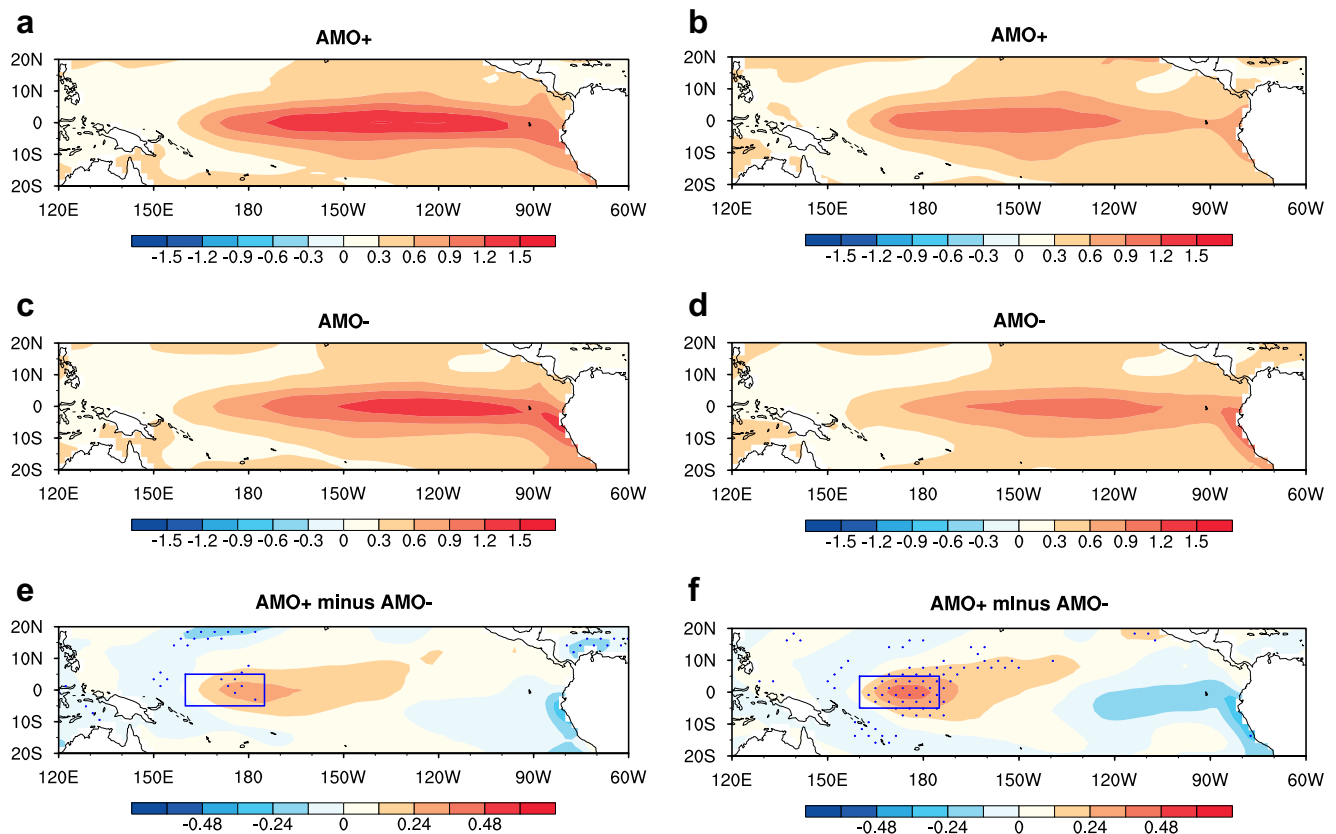
Fig. 5 | Observed differences in El Niño-Southern Oscillation patterns between the positive and negative Atlantic Multidecadal Oscillation (AMO). a, b The standard deviations of (**a**) November–January (NDJ) and (**b**) January–March (JFM) interannual sea surface temperature anomalies (°C) over the tropical Pacific in the positive phase of the AMO during 1999–2018. **c, d** As in (**a**, **b**), but in the negative phase of the AMO during 1960–1998. **e, f** Differences of the standard deviations between the positive and negative AMO. Stippling indicates the differences that are statistically significant at the 90% confidence level using a *F*-test. The blue boxes denote the Niño-4W region (5°S–5°N, 160°E–175°W) in equatorial western-central Pacific.

The present study is dedicated to examine the decadal variation of Ningaloo Niño/Niña strength, the long-term trend caused by external forcing thus has already been removed in our analyses to avoid contamination. But the long-term changes in Ningaloo Niño/Niña strength could be an interesting topic. Here, we show the long-term trends in Ningaloo Niño/Niña amplitude derived from two different SST datasets (Supplementary Fig. 20). Unfortunately, the results show large discrepancies between different observations, which make it difficult to ascertain the influence of external forcing on Ningaloo Niño/Niña amplitude. Further investigations into this aspect with long-term model simulations may help determine the role of external forcing.

The time-varying strength of Ningaloo Niño/Niña caused by AMO could have far-reaching implications in view of its substantial climate and socioeconomic impacts. This is preliminarily demonstrated by comparing the climate impacts of Ningaloo Niño during different AMO phases in both observations and model simulations (Supplementary Figs. 21 and 22). The simulated results are consistent with the observations in spatial pattern, but with a weaker intensity. During the positive AMO when Ningaloo Niño is strengthened, the Ningaloo Niño events tend to induce strong cyclonic circulation in the Southeast Indian Ocean, and intense precipitation anomalies over the Northwest and Southeast Australia. In contrast, the influences of Ningaloo Niño during negative AMO are found to be much weaker than that during positive AMO. Those results indicate that stronger Ningaloo Niño/Niña events during positive AMO correspond to enhanced climate impacts. Moreover, the AMO phase transitions may influence the predictability of Ningaloo Niño/Niña. As Ningaloo Niño events related to ENSO are demonstrated to be

easier to predict than those ENSO independent events[51], Ningaloo Niño/Niña is expected to be more predictable during the positive AMO when ENSO–Ningaloo Niño/Niña relationship is strengthened (Supplementary Fig. 23). In this sense, the AMO phase transitions could affect both the climate impacts and predictability of Ningaloo Niño/Niña. However, the AMO is found to be underestimated in most state-of-the-art coupled general circulation models[52–54]. Improving the simulation of AMO in coupled climate models may help improve the Ningaloo Niño/Niña related climate predictions.

Methods

Observational datasets
The global SST data is primarily based on the latest National Oceanic and Atmospheric Administration Extended Reconstructed SST version 5 (ERSST v5) during 1920–2018[55]. Also, the merged Hadley-OI SST and COBE SST data sets covering the same period are employed to test the reliability of the results[56,57]. Monthly atmospheric reanalysis data is provided by Japanese 55-year Reanalysis (JRA-55) covering 1958–2018, which is the longest third-generation reanalysis that uses the full observing system[58]. The ocean dataset used is primarily from the Simple Ocean Data Assimilation (SODA) version 2.2.4 for 1920–2010[59], which is extended from 2011 to 2018 using the Global Ocean Data Assimilation System[60]. All anomalies are calculated as the deviations from the 1981–2010 climatology. The long-term linear trends in variables are removed by a least squares method. An 11-year running mean is applied to extract the decadal signals. The interannual anomalies of variable fields and indices in observations are obtained by subtracting the low-frequency components, which are estimated by the 11-year (132-month) running means.
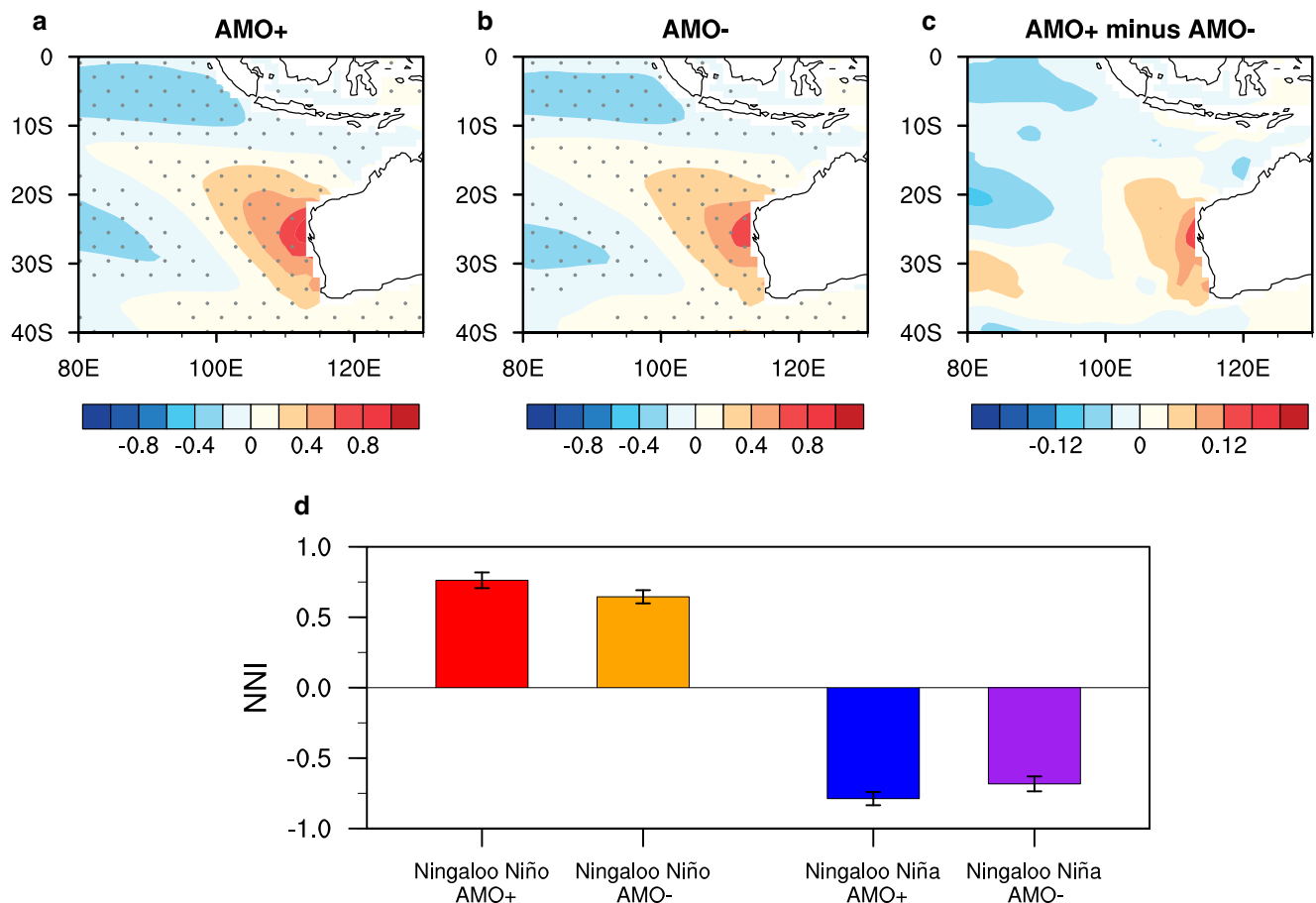
Fig. 6 | Simulated influence of the Atlantic Multidecadal Oscillation (AMO) on Ningaloo Niño/Niña strength. a The regression of interannual January–March (JFM) SST anomalies (°C) onto the normalized Ningaloo Niño/Niña index (NNI) for AMO+ simulations in idealized Atlantic pacemaker experiment based on the EC-Earth3 Earth System Model. **b** As in (**a**), but for AMO− simulations. **c** Difference of the regression patterns between the AMO+ and AMO− simulations. Stippling indicates the regressions that are statistically significant at the 95% confidence level. **d** Composite JFM NNI (bar; °C) for AMO+/Ningaloo Niño (red), AMO−/Ningaloo Niño (orange), AMO+/Ningaloo Niña (blue) and AMO−/Ningaloo Niña (purple) in idealized Atlantic pacemaker experiments. The Ningaloo Niño (Niña) events are selected if the JFM NNI is greater (less) than 0.6 (−0.6) standard deviation in each experiment. Error bars indicate the 90% confidence intervals.

Climate indices

Following previous studies, the Ningaloo Niño/Niña index (NNI) is defined as the areal averaged SST anomalies over 22°–28°S, 108°–116°E[8,12,61]. The Niño-4W index, defined as the mean SST anomalies over 5°S–5°N, 160°E–175°W, is used to measure ENSO in present study[16,17,20]. The adoption of this ENSO index is because Ningaloo Niño/Niña is more closely related to SST anomalies over the equatorial western-central Pacific (Supplementary Fig. 2). To focus on the Ningaloo Niño case, the Niño-4W index used in this study is reversed in sign (multiplied by −1). The ENSO Modoki index (EMI) is defined as EMI = [SSTA]$_A$− 0.5 × [SSTA]$_B$−0.5 × [SSTA]$_C$, where the brackets represent the areal averaged SST anomalies over region A (10°S–10°N, 165°E–140°W), B (15°S–5°N, 110°W–70°W), and C (10°S–20°N, 125°E–145°E)[62]. To better focus on their interannual variability, the low-frequency components in NNI, Niño-4W index and EMI are removed. The AMO index is defined as the area-averaged annual SST anomalies over the North Atlantic basin (0°–70°N, 70°W–0°). The IPO index is calculated as the difference between the annual SST anomalies averaged over the central equatorial Pacific (10°S–10°N, 170°E–90°W) and the average of the SST anomalies in the northwest Pacific (25°–45°N, 140°E–145°W) and southwest Pacific (50°–15°S, 150°E–160°W)[63]. The average of monthly data from July to June of the next year is used as the annual mean in present study.

Significance test

The statistical significance of the differences between the means is assessed using a two-tailed Student t-test. The significance of the differences between the standard deviation is measured based on a two-tailed F-test. The significance of the regressions and correlations is determined using a two-tailed Student t-test. Especially, for significance test of decadal-scale correlations, the effective degrees of freedom are calculated based on the method introduced by Bretherton et al.[64].

Model and experiments

Due to limited length of observations, the idealized Atlantic pacemaker experiment based on EC-Earth3 Earth System Model is further employed to verify the trans-basin influence of AMO on Ningaloo Niño/Niña. The experiment, as a part of the Decadal Climate Prediction Project (DCPP) contribution to sixth Coupled Model Intercomparison Project (CMIP6), is run with time-independent spatial pattern corresponding to the observed AMO SST anomalies imposed on model climatology over the North Atlantic basin (10°–65°N), while the rest of the model evolve freely. To present instability, a buffer zone of 8° is set at the edge of the nudging area. A set of 32-member ensemble simulations are run for AMO+ and AMO− respectively, by restoring North Atlantic SST to positive (negative) AMO pattern superimposed on model climatological SST. To avoid the presence of drift, each
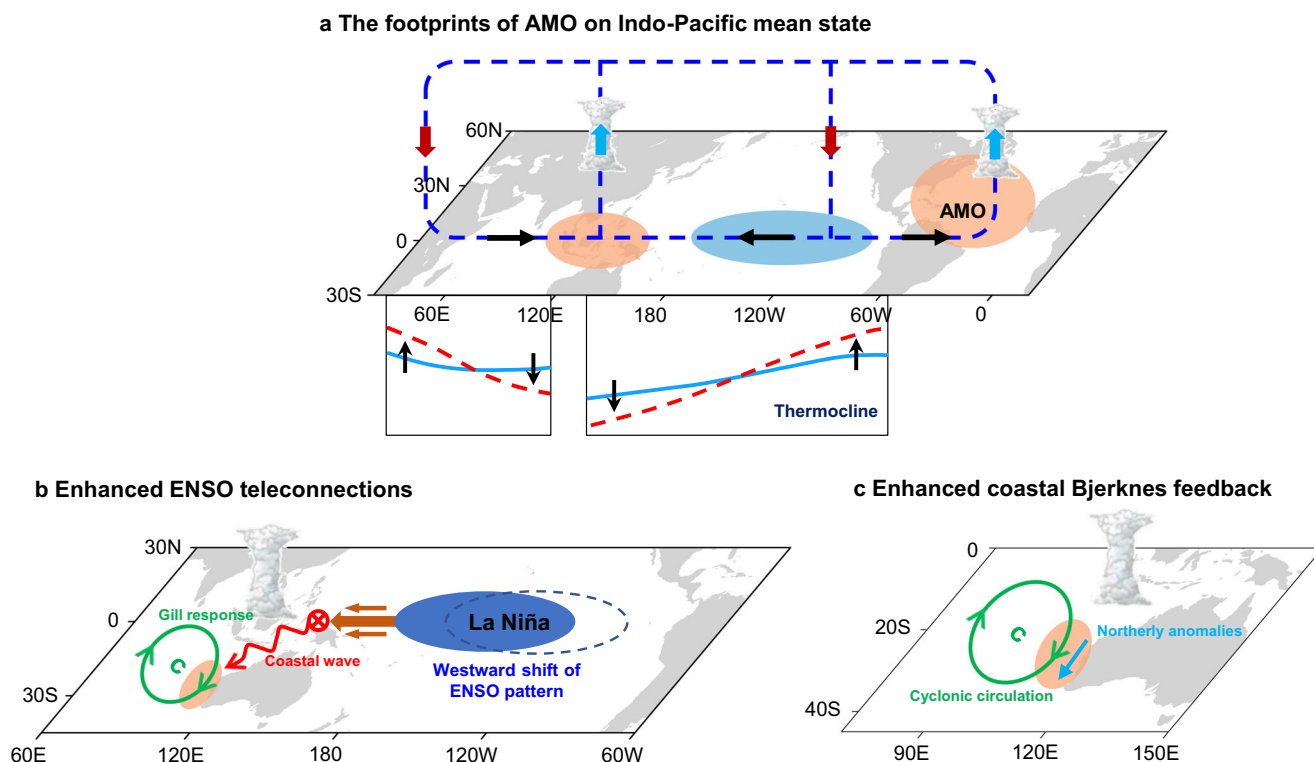
a The footprints of AMO on Indo-Pacific mean state

b Enhanced ENSO teleconnections

c Enhanced coastal Bjerknes feedback

Fig. 7 | Schematic representation of mechanisms behind the Atlantic Multidecadal Oscillation (AMO) modulation of Ningaloo Niño/Niña strength. a The tropical Atlantic warming associated with the positive AMO leads to mean sea surface temperature (SST) cooling over the equatorial central Pacific and mean SST warming in the tropical eastern Indian Ocean through atmospheric Walker circulation. **b** Those mean state changes lead to the westward shift of El Niño-Southern Oscillation (ENSO) pattern and modify the climate sensitivity to ENSO forcing, which enhance ENSO atmospheric and oceanic teleconnections to the southeast Indian Ocean, thereby promoting the Ningaloo Niño/Niña amplitude. **c** The mean SST warming over the tropical eastern Indian Ocean makes the atmosphere more unstable and enhances background convection. For this unstable and convection-active state, the atmospheric convection will be more sensitive to underlying SST anomalies, thus leading to enhanced coastal Bjerknes feedback and Ningaloo Niño/Niña strength.

realization is run for 10 years with all external forcing held constant at the pre-industrial values[65,66]. The 32 ensemble members for each experiment are generated by introducing perturbations in initial conditions. The first year of each realization is considered as a spin-up period, and is discarded for the current analyses. The average of AMO+ and AMO− simulations is considered as the corresponding reference state for each ensemble. Moreover, the interannual anomalies of variable fields and indices in simulations are derived by subtracting the low-frequency components in each realization, which are estimated by 5-year running means. By joining 32 ensemble members, a record of 288-year simulations is obtained and analyzed for AMO+ and AMO−.

Data availability

All observational and model datasets that support the findings of this study are freely available. The ERSST data is available at https://psl.noaa.gov/data/gridded/data.noaa.ersst.v5.html. The merged Hadley-OI SST data set is available at https://gdex.ucar.edu/dataset/158_asphilli/file.html. The COBE SST data is available at https://psl.noaa.gov/gridded/data.cobe2.html. The JRA-55 data is available at https://rda.ucar.edu/datasets/d628001/#. The SODA data is available at https://apdrc.soest.hawaii.edu/erddap/griddap/hawaii_soest_c71f_e12b_37f8.html. The GOADS data is available at https://www.esrl.noaa.gov/psd/data/gridded/data.godas.html. The EC-Earth3 idealized Atlantic simulations can be obtained from https://aims2.llnl.gov/search/cmip6/.

Code availability

The data in this study was analyzed with the NCAR Command Language (NCL; https://www.ncl.ucar.edu/). The codes to calculate results are available upon request to the corresponding author J.X.

References

1. Frölicher, T. L. & Laufkötter, C. Emerging risks from marine heat waves. *Nat. Commun.* **9**, 650 (2018).
2. Frölicher, T. L., Fischer, E. M. & Gruber, N. Marine heatwaves under global warming. *Nature* **560**, 360–364 (2018).
3. Oliver, E. C. J. et al. Longer and more frequent marine heatwaves over the past century. *Nat. Commun.* **9**, 1324 (2018).
4. Holbrook, N. J. et al. A global assessment of marine heatwaves and their drivers. *Nat. Commun.* **10**, 2624 (2019).
5. Zinke, J. et al. Corals record long-term Leeuwin current variability including Ningaloo Niño/Niña since 1795. *Nat. Commun.* **5**, 3607 (2014).
6. Zinke, J. et al. Coral record of southeast Indian Ocean marine heatwaves with intensified Western Pacific temperature gradient. *Nat. Commun.* **6**, 8562 (2015).
7. Feng, M., McPhaden, M. J., Xie, S. P. & Hafner, J. La Niña forces unprecedented Leeuwin current warming in 2011. *Sci. Rep.* **3**, 1277 (2013).
8. Kataoka, T., Tozuka, T., Behera, S. & Yamagata, T. On the Ningaloo Niño/Niña. *Clim. Dyn.* **43**, 1463–1482 (2013).
9. Feng, M. et al. Multi-year marine cold-spells off the west coast of australia and effects on fisheries. *J. Marine Syst.* **214**, 103473 (2021).
10. Ding, Y., Chen, L., Lin, P., Liu, H. & Wang, R. Analysis of Ningaloo Niño simulated by two coupled models of FGOALS3. *Deep Sea Res. Part II Top. Stud. Oceanogr.* **194**, 104988 (2021).
11. Zhang, L., Han, W., Li, Y. & Shinoda, T. Mechanisms for generation and development of the Ningaloo Niño. *J. Clim.* **31**, 9239–9259 (2018).

12. Kataoka, T., Masson, S., Izumo, T., Tozuka, T. & Yamagata, T. Can Ningaloo Niño/Niña develop without El Niño–Southern Oscillation? *Geophys. Res. Lett.* **45**, 7040–7048 (2018).

13. Clarke, A. J. & Liu, X. Interannual sea level in the northern and eastern Indian Ocean. *J. Phys. Oceanogr.* **24**, 1224–1235 (1994).

14. Meyers, G. Variation of Indonesian throughflow and the El Niño-southern oscillation. *J. Geophys. Res.* **101**, 12255–12263 (1996).

15. Wang, C. Three-ocean interactions and climate variability: a review and perspective. *Clim. Dyn.* **53**, 5119–5136 (2019).

16. Ding, Y. et al. Emergence of decadal linkage between Western Australian coast and Western–central tropical Pacific. *Nat. Commun.* **15**, 4458 (2024).

17. Feng, M., Zhang, Y., Hendon, H. H., McPhaden, M. J. & Marshall, A. G. Niño 4 west (Niño-4W) sea surface temperature variability. *J. Geophys. Res. Oceans* **126**, e2021JC017591 (2021).

18. Tozuka, T., Kataoka, T. & Yamagata, T. Locally and remotely forced atmospheric circulation anomalies of Ningaloo Niño/Niña. *Clim. Dyn.* **43**, 2197–2205 (2014).

19. Tozuka, T., Feng, M., Han, W., Kido, S., & Zhang, L. The Ningaloo Niño/Niña: mechanisms, relation with other climate modes and impacts. *Trop. Extratrop. Air-Sea Interact.* 207–219 (2021).

20. Marshall, A. G., Hendon, H. H., Feng, M. & Schiller, A. Initiation and amplification of the Ningaloo Niño. *Clim. Dyn.* **45**, 2367–2385 (2015).

21. Xue, J., Luo, J. -J., Yuan, C. & Yamagata, T. Discovery of Chile Niño/Niña. *Geophys. Res. Lett.* **47**, e2019GL086468 (2020).

22. Kido, S., Kataoka, T. & Tozuka, T. Ningaloo Niño simulated in the CMIP5 models. *Clim. Dyn.* **47**, 1469–1484 (2016).

23. Xue, J. et al. Ningaloo Niño/Niña in CMIP6 models: characteristics, mechanisms, and climate impacts. *Geophys. Res. Lett.* **49**, e2022GL099781 (2022).

24. Zhang, L. & Han, W. Impact of Ningaloo Niño on tropical Pacific and an interbasin coupling mechanism. *Geophys. Res. Lett.* **45**, 11300–11309 (2018).

25. Depczynski, M. et al. Bleaching, coral mortality and subsequent survivorship on a West Australian fringing reef. *Coral Reefs* **32**, 233–238 (2013).

26. Pearce, A. & Feng, M. The rise and fall of the "marine heat wave" off Western Australia during the summer of 2010/11. *J. Mar. Syst* **111**, 139–156 (2013).

27. Wernberg, T. et al. An extreme climatic event alters marine ecosystem structure in a global biodiversity hotspot. *Nat. Clim. Change* **3**, 78–82 (2013).

28. Feng, M. et al. Decadal increase in Ningaloo Niño since the late 1990s. *Geophys. Res. Lett.* **42**, 104–112 (2015).

29. Tanuma, N. & Tozuka, T. Influences of the interdecadal Pacific Oscillation on the locally amplified Ningaloo Niño. *Geophys. Res. Lett.* **47**, e2020GL088712 (2020).

30. Enfield, D. B., Mestas-Nunez, A. M. & Trimble, P. J. The Atlantic multidecadal oscillation and its relation to rainfall and river flows in the continental US. *Geophys. Res. Lett.* **28**, 2077–2080 (2001).

31. Sutton, R. T. & Hodson, D. L. R. Atlantic Ocean forcing of North American and European summer climate. *Science* **309**, 115–118 (2005).

32. Knight, J. R., Folland, C. K. & Scaife, A. A. Climate impacts of the Atlantic Multidecadal Oscillation. *Geophys. Res. Lett.* **33**, L17706 (2006).

33. Sun, C., Li, J. P. & Zhao, S. Remote influence of Atlantic multidecadal variability on Siberian warm season precipitation. *Sci. Rep.* **5**, 16853 (2015).

34. Goswami, B. N., Madhusoodanan, M. S., Neema, C. P. & Sengupta, D. A physical mechanism for North Atlantic SST influence on the Indian summer monsoon. *Geophys. Res. Lett.* **33**, L02706 (2006).

35. Lu, R. Y., Dong, B. W. & Ding, H. Impact of the Atlantic multidecadal oscillation on the Asian summer monsoon. *Geophys. Res. Lett.* **33**, L24701 (2006).

36. Xue, J. et al. Multidecadal variation of northern hemisphere summer monsoon forced by the SST inter-hemispheric dipole. *Environ. Res. Lett.* **17**, 044033 (2022).

37. Zhang, R. & Delworth, T. L. Impact of the Atlantic Multidecadal Oscillation on North Pacific climate variability. *Geophys. Res. Lett.* **34**, L23708 (2007).

38. Sun, C. et al. Western tropical Pacific multidecadal variability forced by the Atlantic multidecadal oscillation. *Nat. Commun.* **8**, 15998 (2017).

39. Kucharski, F. et al. Atlantic forcing of Pacific decadal variability. *Clim. Dyn.* **46**, 2337–2351 (2015).

40. Li, X., Xie, S.-P., Gille, S. T. & Yoo, C. Atlantic-induced pan-tropical climate change over the past three decades. *Nat. Clim. Change* **6**, 275–279 (2015).

41. Meehl, G. A. et al. Atlantic and Pacific tropics connected by mutually interactive decadal-timescale processes. *Nat. Geosci.* **14**, 36–42 (2021).

42. Kucharski, F. et al. A Gill–Matsuno-type mechanism explains the tropical Atlantic influence on African and Indian monsoon rainfall. *Quart. J. Roy. Meteor. Soc* **135**, 569–579 (2009).

43. Xue, J., Luo, J.-J., Zhang, W. & Yamagata, T. ENSO–IOD inter-basin connection is controlled by the Atlantic Multidecadal Oscillation. *Geophys. Res. Lett.* **49**, e2022GL101571 (2022).

44. Liu, Y., Li, Z., Cai, W., Lin, X. & Yang, J.-C. Weakened ENSO-Ningaloo Niño/Niña teleconnection under greenhouse warming. *Geophys. Res. Lett.* **48**, e2020GL091326 (2021).

45. Dong, B. & Dai, A. The influence of the interdecadal Pacific oscillation on temperature and precipitation over the globe. *Clim. Dyn.* **45**, 2667–2681 (2015).

46. Meehl, G. et al. Contribution of the Interdecadal Pacific Oscillation to twentieth-century global surface temperature trends. *Nat. Clim. Change* **6**, 1005–1008 (2016).

47. Xiang, B., Wang, B. & Li, T. A new paradigm for the predominance of standing Central Pacific warming after the late 1990s. *Clim. Dyn.* **41**, 327–340 (2013).

48. Chung, P.-H. & Li, T. Interdecadal relationship between the mean state and El Niño types. *J. Clim.* **26**, 361–379 (2013).

49. Yu, J. Y. et al. Linking emergence of the central Pacific El Niño to the Atlantic multidecadal oscillation. *J. Clim.* **28**, 651–662 (2015).

50. Lübbecke, J. F. & McPhaden, M. J. Assessing the 21st century shift in ENSO variability in terms of the Bjerknes stability index. *J. Clim.* **27**, 2577–2587 (2014).

51. Doi, T., Behera, S. K. & Yamagata, T. Predictability of the Ningaloo Niño/Niña. *Sci. Rep.* **3**, 2892 (2013).

52. Zhang, L. & Wang, C. Multidecadal North Atlantic sea surface temperature and Atlantic Meridional Overturning Circulation variability in CMIP5 historical simulations. *J. Geophys. Res. Oceans* **118**, 5772–5791 (2013).

53. Murphy, L. N., Bellomo, K., Cane, M. & Clement, A. The role of historical forcings in simulating the observed Atlantic multidecadal oscillation. *Geophys. Res. Lett.* **44**, 2472–2480 (2017).

54. Xia, S. et al. Simulation evaluation of AMO and PDO with CMIP5 and CMIP6 models in historical experiment. *Adv. Earth Sci.* **36**, 58e68 (2021).

55. Huang, B. et al. Extended reconstructed sea surface temperature, version 5 (ERSSTv5): upgrades, validations, and intercomparisons. *J. Clim.* **30**, 8179–8205 (2017).

56. Hurrell, J. et al. A new sea surface temperature and sea ice boundary dataset for the Community Atmosphere Model. *J. Clim* **21**, 5145–5153 (2008).

57. Ishii, M., Shouji, A., Sugimoto, S. & Matsumoto, T. Objective analyses of sea-surface temperature and marine meteorological variables for the 20th century using ICOADS and the Kobe collection. *Int. J. Climatol.* **25**, 865–879 (2005).

58. Kobayashi, S. et al. The JRA-55 reanalysis: general specifications and basic characteristics. *J. Meteorol. Soc. Jpn* **93**, 5–48 (2015).

59. Carton, J. A. & Giese, B. S. A reanalysis of ocean climate using Simple Ocean Data Assimilation (SODA). *Mon. Weather Rev.* **136**, 2999–3017 (2008).

60. Behringer, D. W. & Xue Y. Evaluation of the global ocean data assimilation system at NCEP: the Pacific Ocean. In *Eighth Symposium on Integrated Observing and Assimilation Systems for Atmosphere, Oceans, and Land Surface,* AMS 84th Annual Meeting (AMS, 2004).

61. Guo, Y., Li, Y., Wang, F., Wei, Y. & Rong, Z. Processes controlling sea surface temperature variability of Ningaloo Niño. *J. Clim.* **33**, 4369–4389 (2020).

62. Ashok, K., Behera, S. K., Rao, S. A., Weng, H. & Yamagata, T. El Niño Modoki and its possible teleconnection. *J. Geophys. Res.* **112**, C11007 (2007).

63. Henley, B. J. et al. A tripole index for the interdecadal Pacific oscillation. *Clim. Dyn.* **45**, 3077–3090 (2015).

64. Bretherton, C. S., Widmann, M., Dymnikov, V. P., Wallace, J. M. & Bladé, I. The effective number of spatial degrees of freedom of a time-varying field. *J. Clim.* **12**, 1990–2009 (1999).

65. Döscher, R. et al. The EC-Earth3 earth system model for the climate model intercomparison project 6. *Geosci. Model Dev.* **15**, 2973–3020 (2022).

66. Boer, G. J. et al. The decadal climate prediction project (DCPP) contribution to CMIP6. *Geosci. Model Dev.* **9**, 3751–3777 (2016).

Acknowledgements

Author contributions

J.X. conceived the study, performed the analyses, prepared the figures and wrote the initial manuscript. W.Z., T.Y., and J.L. contributed to organize and revise the manuscript. Y.Z. helped improve the manuscript. H.Z. helped with the data collections. C.S. provided discussions.

Competing interests

The authors declare no competing interests.

Additional information

Supplementary information The online version contains supplementary material available at https://doi.org/10.1038/s41467-025-57160-7.

Correspondence and requests for materials should be addressed to Jiaqing Xue or Wenjun Zhang.

Peer review information *Nature Communications* thanks the anonymous reviewers for their contribution to the peer review of this work. A peer review file is available.

Reprints and permissions information is available at http://www.nature.com/reprints

Publisher's note Springer Nature remains neutral with regard to jurisdictional claims in published maps and institutional affiliations.